催 化 学 报
2012 *Chinese Journal of Catalysis* Vol. 33 No. 1

文章编号: 0253-9837(2012)01-0106-08 国际版 DOI: 10.1016/S1872-2067(10)60281-1 研究论文: 106~113

紫外拉曼光谱研究 $FeAlPO_4$-5 分子筛的合成机理

郭 强[1,2], 范峰滔[1,a], 郭美玲[1,2], 冯兆池[1], 李 灿[1,b]

[1]中国科学院大连化学物理研究所催化基础国家重点实验室, 辽宁大连 116023

[2]中国科学院研究生院, 北京 100049

摘要: 利用紫外共振拉曼光谱和紫外-可见漫反射光谱对不同铁含量的 $FeAlPO_4$-5 分子筛进行了研究. 结果表明, $FeAlPO_4$-5 分子筛的骨架铁有 4 个特征的拉曼谱峰, 分别位于 630, 1060, 1140 和 1210 cm^{-1}. 当凝胶中 Al/Fe 比小于 380 时, 只有一部分铁离子可以进入分子筛形成四配位的骨架铁物种; 而另一部分则以骨架外六配位的铁物种存在, 其特征拉曼谱峰位于 285 cm^{-1}. 结合紫外拉曼光谱、紫外-可见漫反射光谱和 X 射线衍射研究了 Al/Fe 比为 760 时 $FeAlPO_4$-5 分子筛的晶化过程. 结果发现, 在分子筛晶化前, 铁物种以六配位的形式存在, 它为分子筛前体中的一维链状磷酸铝添加了一个惰性端基, 六配位的 Fe-O 键不利于它与其它磷酸铝物种发生反应; 当分子筛开始晶化时, 带有铁离子端基的磷酸铝链与其它磷酸铝链进一步反应形成分子筛骨架. 同时, 六配位的铁离子和邻近的磷酸铝物种反应转化为四配位的骨架铁物种.

关键词: 铁; $AlPO_4$-5 分子筛; 紫外拉曼光谱; 共振拉曼效应; 合成机理

中图分类号: O643 **文献标识码**: A

收稿日期: 2011-08-05. 接受日期: 2011-09-13.

[a]通讯联系人. 电话: (0411)84379302; 传真: (0411)84694447; 电子信箱: ftfan@dicp.ac.cn

[b]通讯联系人. 电话: (0411)84379070; 传真: (0411)84694447; 电子信箱: canli@dicp.ac.cn

基金来源: 国家自然科学基金 (21003122).

本文的英文电子版(国际版)由Elsevier出版社在ScienceDirect上出版(http://www.sciencedirect.com/science/journal/18722067).

UV Raman Spectroscopic Studies on the Mechanism of $FeAlPO_4$-5 Synthesis

GUO Qiang[1,2], FAN Fengtao[1,a], GUO Meiling[1,2], FENG Zhaochi[1], LI Can[1,b]

[1]*State Key Laboratory of Catalysis, Dalian Institute of Chemical Physics, Chinese Academy of Sciences, Dalian 116023, Liaoning, China*

[2]*Graduate University of Chinese Academy of Sciences, Beijing 100049, China*

Abstract: $FeAlPO_4$-5 samples with various iron contents were investigated by UV resonance Raman spectroscopy and UV-Vis spectroscopy. The Raman spectra of $FeAlPO_4$-5 show four feature bands related to the framework iron at 630, 1060, 1140, and 1210 cm^{-1} when excited by 266 nm laser. It is found that only part of ferric ions could enter into the framework, while the others exist in the extra-framework in the form of six-coordinated state. This kind of iron gives characteristic Raman band at 285 cm^{-1}. Combined with UV resonance Raman spectroscopy, UV-Vis spectroscopy, and X-ray diffraction, the crystallization process of $FeAlPO_4$-5 (Al/Fe = 760) was studied. It is found that, in the early stages of the crystallization, the iron species exist in the form of six-coordinated state while attached to the end of the 1-dimensional $AlPO_4$ chain. The Fe–O bonds in the six-coordinated state hamper the crystallization of $AlPO_4$. The crystallization of the $FeAlPO_4$-5 began when the reaction between the 1-dimensional $AlPO_4$ chains occurred. At the same time, the six-coordinated ferric ions converted to the tetrahedral iron.

Key words: iron; $AlPO_4$-5 zeolite; UV Raman spectroscopy; resonance Raman effect; synthesis mechanism

Received 5 August 2011. Accepted 13 September 2011.

[a]*Corresponding author. Tel: +86-411-84379302; Fax: +86-411-84694447; E-mail: ftfan@dicp.ac.cn*

[b]*Corresponding author. Tel: +86-411-84379070; Fax: +86-411-84694447; E-mail: canli@dicp.ac.cn*

This work was supported by the National Natural Science Foundation of China (21003122).

English edition available online at Elsevier ScienceDirect (http://www.sciencedirect.com/science/journal/18722067).

磷酸铝分子筛 $AlPO_4$-*n* 的合成是分子筛合成历史上的一个重要里程碑, 将杂原子引入骨架可以形

成具有多种功能的微孔分子筛[1]. 含铁分子筛在很多重要的催化反应, 特别是氧化-还原反应中, 显示出其独特的催化性能. 其中 Fe-ZSM-5 分子筛因在环境催化、选择性氧化等方面的优异催化性能而引起了人们极大的兴趣. 阐明这些不同反应铁活性位的性质一直是有关 Fe-ZSM-5 催化体系的研究重点. 普遍的观点认为, 其中的活性位更有可能是非骨架的铁物种, 而不是骨架位的铁物种[2~8]. 与硅铝分子筛不同, 在磷酸铝分子筛骨架四配位的铁物种被认为是反应活性中心. Ren 等[9]在研究石英相的 $FePO_4$ 时发现, 四配位的三价铁在苯羟化反应中有很好的选择性. 在铁取代的 AlPO-5 分子筛中, 铁通常是以四配位形式存在的, 而它们在分子氧的存在下被认为是氧化反应的活性中心[10,11]. Shiju 等[12]在用 XANES 研究铁取代的 $AlPO_4$-5 分子筛时发现, 分子筛骨架中四配位的铁物种是苯羟化的活性中心. Mul 课题组的研究表明, 骨架中四配位的三价铁物种只有还原成二价铁才能成为 N_2O 分解的活性中心[13]. 综上所述, 精确表征铁物种在 $FeAlPO_4$-5 中存在的状态及其合成规律对理解催化反应活性中心以及提高反应活性位浓度非常重要. 但是, 由于微孔分子筛骨架可以引入的过渡金属的量通常很低(2%)[14], 所以很难得到有关分子筛中过渡金属原子的信息. 在过去十几年中, 本课题组的研究表明, 紫外拉曼光谱能够解决传统拉曼光谱技术在表征分子筛催化剂时遇到的荧光问题, 是一种强有力的表征微孔和介孔材料的手段[15,16]. 特别是, 利用紫外拉曼共振效应, 可以选择性、高灵敏地得到微孔和介孔材料中过渡金属原子的信息, 同时给出含过渡金属原子在分子筛晶化的不同阶段铁物种的配位状态[17~24].

本文利用紫外共振拉曼光谱和紫外-可见漫反射光谱对不同铁含量的 $FeAlPO_4$-5 分子筛以及分子筛晶化过程中铁物种的变化进行了研究. 以期为理解过渡金属取代的微孔分子筛合成机理及指导合成新型过渡金属取代的微孔分子筛提供理论依据.

1 实验部分

1.1 分子筛的制备

将磷酸 (天津市科密欧化学试剂开发中心) 和去离子水混合均匀后, 向混合液中加入拟薄水铝石 (山东淄博铝厂), 搅拌 120 min 后逐滴加入三乙胺 (天津市科密欧化学试剂开发中心) 继续搅拌均匀, 最后加入一定量的 $FeCl_3$ (天津市科密欧化学试剂开发中心) 溶液后搅拌 120 min, 即得到凝胶. 将其装入带有聚四氟乙烯的不锈钢反应釜中, 在 140 ºC 下静态晶化 2160 min. 晶化产物经过滤、洗涤后于 80 ºC 下干燥 720 min, 即得到分子筛原粉.

不同晶化时间 $FeAlPO_4$-5 分子筛的制备: 将上述搅拌好的凝胶转入不锈钢反应釜中, 于 140 ºC 分别静态晶化不同时间. 晶化结束后, 将反应釜淬冷, 产物经过滤、洗涤, 于 80 ºC 干燥 720 min, 即得到分子筛原粉.

1.2 样品的表征

X 射线衍射 (XRD) 实验在 DINT D/max-2500/PC 型 X 射线衍射仪 (日本 Rigaku 公司) 上进行. Cu K_α 射线源, Ni 滤波, 管电流 200 mA, 管电压 40 kV, 扫描范围 $2\theta = 5^o$~40^o, 扫描速率 5^o/min. 样品的紫外拉曼光谱在自行设计的紫外拉曼光谱仪上进行测定. 其分光系统采用 SPEX Triplemate 1877D 型三光栅单色仪 (Jobin-Yvon 公司), 检测器使用液氮冷却的 Spectrum One CCD 2000 型光电耦合检测器, 激发光源采用 IK-3351-G 型 He-Cd 激光器 (325 nm) 和通过对 DPSS 532 Model 200 激光器产生的 532 nm 的激光倍频产生的 266 nm 的激光.

2 结果与讨论

2.1 不同 Al/Fe 比的 $FeAlPO_4$-5 样品的 XRD 谱和紫外-可见漫反射光谱

图 1(a) 为不同 Al/Fe 比的 $FeAlPO_4$-5 分子筛的 XRD 谱. 可以看出, 所有合成样品均具有 AFI 结构特征的衍射峰. 图 1(b) 为不同铁含量 $FeAlPO_4$-5 分子筛的紫外-可见漫反射谱. 可以看出, 位于 260 nm 处出现一个强的吸收带, 归属于骨架氧到铁的荷电跃迁, 它们是骨架孤立四配位 Fe^{3+} 的特征谱峰. 随着样品中铁含量的增加, 在 290 nm 左右逐渐出现肩峰, 可以归属为分子筛中高度隔离的六配位 Fe^{3+} 复合物.

2.2 $AlPO_4$-5 和 Al/Fe 比的 $FeAlPO_4$-5 样品的紫外拉曼光谱

图 2(a) 给出了 $AlPO_4$-5 和不同 Al/Fe 比的 $FeAlPO_4$-5 分子筛样品用 266 nm 作为激发线的紫外

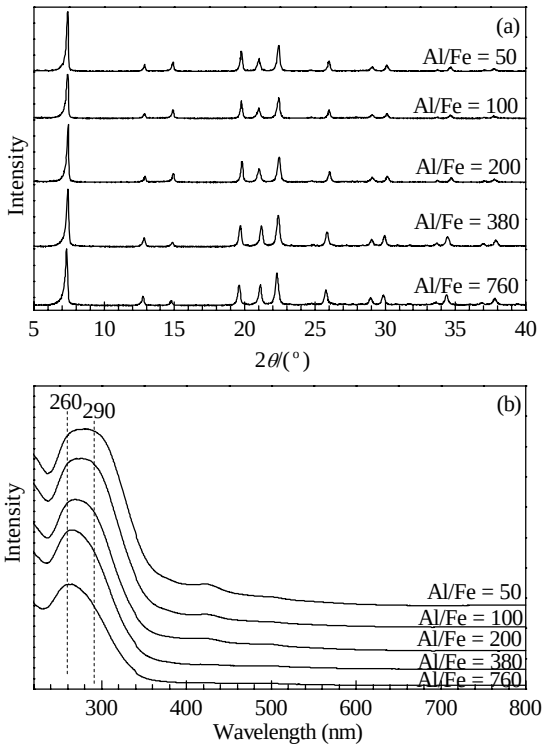

图 1 不同 Al/Fe 比的 $FeAlPO_4$-5 样品的 XRD 谱和 UV-Vis 谱

Fig. 1. XRD patterns (a) and UV-Vis spectra (b) of $FeAlPO_4$-5 samples with different Al/Fe ratios.

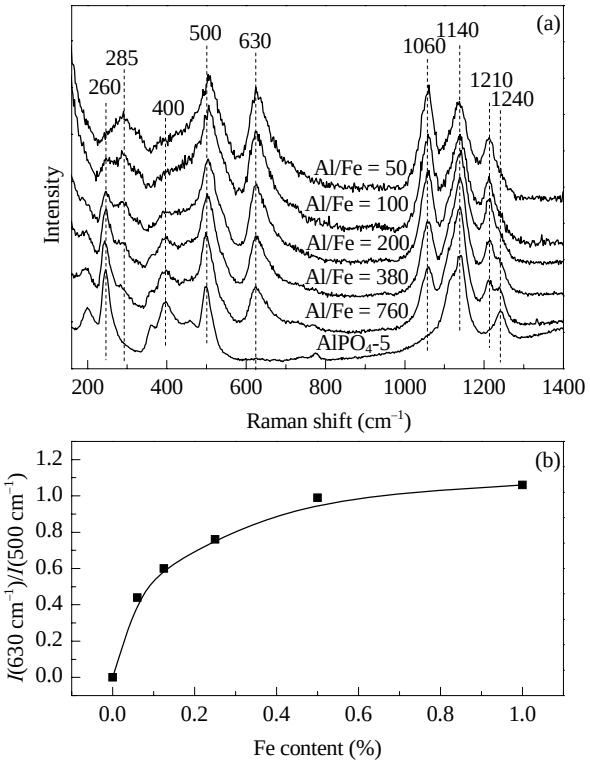

图 2 不同 Al/Fe 比的 $FeAlPO_4$-5 样品的紫外拉曼光谱 (λ_{ex} = 266 nm) 以及 I(630 cm^{-1})/I(500 cm^{-1}) 与样品中铁含量的关系曲线

Fig. 2. Raman spectra (λ_{ex} = 266 nm) (a) and relation between I(630 cm^{-1})/I(500 cm^{-1}) value and Fe content (b) of $FeAlPO_4$-5 samples H.

拉曼光谱. 266 nm 激发线与 $FeAlPO_4$-5 分子筛中 260 nm 的荷电跃迁带能量非常接近. 除了 AFI 分子筛骨架的特征谱峰 (260, 400, 500, 1140 和 1240 cm^{-1}) 外[25], 含铁分子筛的紫外拉曼光谱在 630, 1060 和 1210 cm^{-1} 出现了新的谱峰. 我们曾利用周期场密度泛函理论对这些谱峰进行了详细的归属: 630 cm^{-1} 归属为 $Fe(OP)_4$ 的全对称伸缩振动, 1060 cm^{-1} 归属为 $Fe(OP)_4$ 的非全对称伸缩振动, 1210 cm^{-1} 归属为与 FeO_4 四面体邻近的 P–O–Al 的不对称伸缩振动引发的 FeO_4 的全对称伸缩振动, 而 FeO_4 的全对称伸缩振动可能由于和分子筛骨架位于同一位置 (1210 cm^{-1}) 而无法明确区分出来[19,26,27]. 随着铁含量的增加, 这些拉曼谱峰的强度增强. 同时, 在 285 cm^{-1} 出现一个新的拉曼谱峰, 且随着铁含量的增加而逐渐增强. 该谱峰可归属于来自六配位的 Fe–O 的拉曼振动[28]. 结合紫外-可见漫反射光谱的结果, 可以推断该谱峰归属于高度隔离的六配位 Fe^{3+}复合物. 由此可见, 铁含量非常低时, $FeAlPO_4$-5 分子筛中即已出现了非骨架的铁物种, 且随着铁含量的增加逐渐增加.

图 2(b) 为 630 cm^{-1} 谱峰与 500 cm^{-1} 谱峰强度的比值与 $FeAlPO_4$-5 分子筛中铁含量之间的关系曲线. 可以看出, 该比值并不是线性增加的, 其增加的速率随铁含量的增加而降低. 这表明在高铁含量时, 铁原子很难全部进入分子筛骨架. 此外, 该结果也和紫外拉曼光谱以及紫外-可见漫反射光谱中出现六配位 Fe^{3+} 物种的特征谱带一致. 值得注意的是, 极低铁含量时 $FeAlPO_4$-5 分子筛中已经出现了位于 285 cm^{-1} 处的非骨架六配位铁物种.

2.3 $FeAlPO_4$-5 晶化过程的 XRD 谱和紫外-可见漫反射光谱

图 3(a) 给出了 $FeAlPO_4$-5 (Al/Fe = 760) 不同晶化时间的 XRD 谱. 可以看出, 晶化 120 min 时合成体系中形成了一些具有 AFI 结构的小晶体. 然而, 在 2θ = 14.5°和 28° 处的宽峰表明, 此时存在大量的拟薄水铝石; 至 2160 min 后, 可得到高度结晶的 $FeAlPO_4$-5 分子筛.

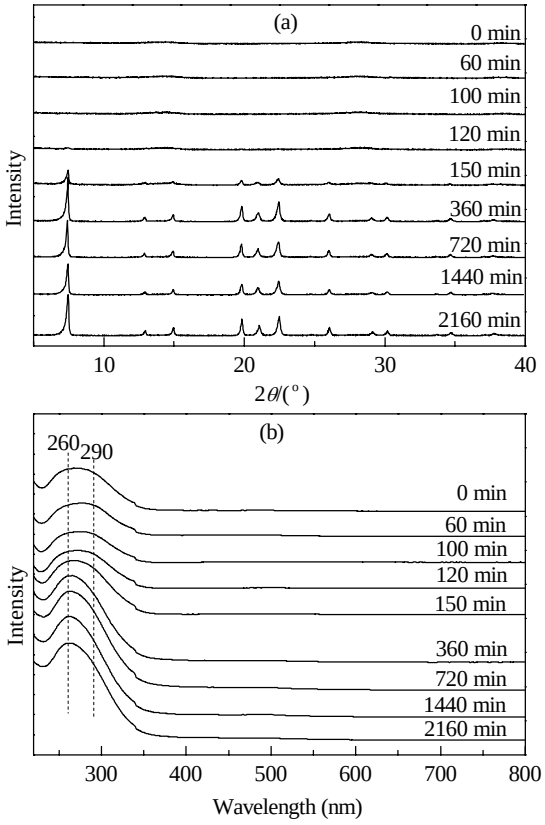

图 3 不同晶化时间的 $FeAlPO_4$-5 的 XRD 谱和紫外-可见漫反射光谱

Fig. 3. XRD patterns (a) and UV-Vis spectra (b) of $FeAlPO_4$-5 crystallized for different time.

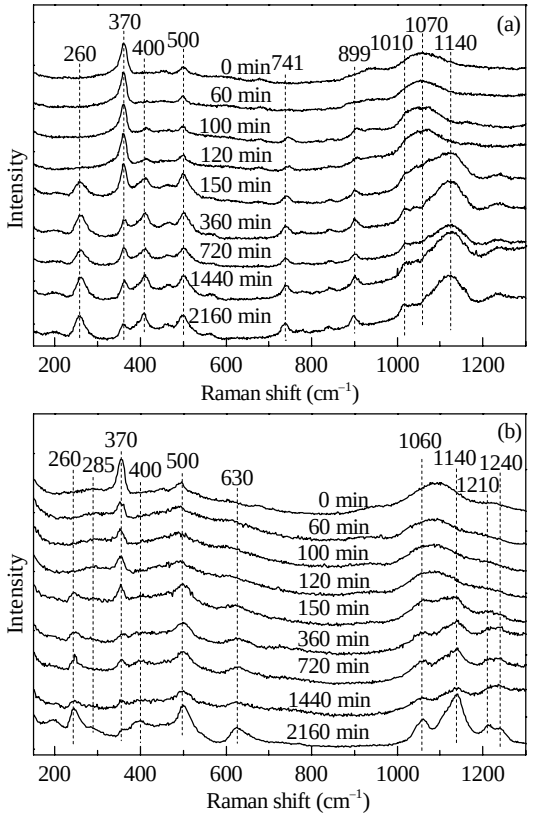

图 4 不同晶化时间时 $FeAlPO_4$-5 (Al/Fe = 760) 的紫外拉曼光谱

Fig. 4. Raman spectra of $FeAlPO_4$-5 crystallized for different time. (a) λ_{ex} = 325 nm; (b) λ_{ex} = 266 nm.

图 3(b) 给出了 $FeAlPO_4$-5 (Al/Fe = 760) 样品在不同合成阶段的紫外-可见漫反射光谱. 可以看出, 合成前体于 275 nm 左右处出现一个非常宽的谱带. 这表明前体中含有六配位的 Fe^{3+} 物种, 且随着晶化的进行而逐渐增强且尖锐. 晶化 2160 min 的样品在 260 nm 处出现很强的荷电跃迁谱带. 结果表明, 前体含有六配位的 Fe^{3+}物种, 经过水热晶化过程, 逐渐转化为四配位的骨架铁物种.

2.4 $FeAlPO_4$-5 晶化过程的紫外拉曼光谱

图 4(a) 给出了不同晶化时间时 $FeAlPO_4$-5 (325 nm 激发) 的紫外拉曼光谱. 初始前体分别于 370, 500 和 1070 cm^{-1} 处出现特征谱峰, 其中前两者归属于薄水铝石中的 AlO_6 物种; 而后者归属于无定形的 Al-O-P 物种. 随着反应的进行, 前两者谱峰逐渐减弱, 而后者谱峰逐渐向高波数移动, 表明前体中的铝逐渐参与反应, 逐步形成规整的结构. 反应至 1.7 h 时, 于 741, 899 和 1010 cm^{-1} 处出现拉曼谱峰, 可归属于质子化的模板剂. 这表明随着反应的进行, 模板剂逐渐和凝胶作用而进入了分子筛孔道中. 当反应进行到 150 min 时, 在 260, 400, 500 和 1130 cm^{-1} 出现谱峰, 前三者归属于分子筛孔道、六元环和四元环的呼吸振动, 表明样品已经开始晶化. 位于 1140 cm^{-1} 处的谱峰归属于 AFI 结构中 AlO_4 和 PO_4 四面体中的 Al-O-P 的反对称伸缩振动. 这一谱峰的出现也是分子筛晶化的标志.

为了研究 $FeAlPO_4$-5 分子筛晶化过程中铁物种的变化, 图 4(b) 给出了不同晶化时间时 $FeAlPO_4$-5 分子筛在除去模板剂后 266 nm 激发的紫外拉曼光谱. 可以看出, 在反应前 120 min 时, 由 266 nm 激发的紫外拉曼光谱和由 325 nm 激发的紫外拉曼光谱相似: 位于 370 和 500 cm^{-1} 处的 AlO_6 的谱峰和位于 1070 cm^{-1} 处的无定形 Al–O–P 物种的谱峰. 除此之外, 在 285 cm^{-1} 处有一弱宽峰. 在分子筛开始晶化 (150 min) 后, 出现分子筛骨架的谱峰: 260, 400, 500 和 1130 cm^{-1}, 同时出现了位于 630, 1060 和 1210 cm^{-1} 处骨架铁的拉曼谱峰, 并且随着晶化的

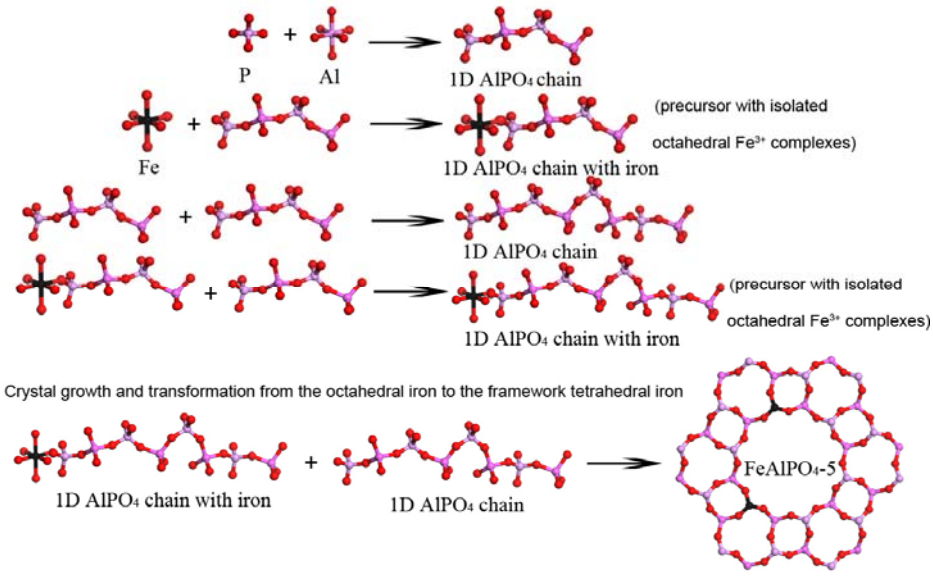

图式 1 FeAlPO$_4$-5 分子筛晶化过程中铁物种的变化

Scheme 1. The evolution of the iron species during the crystallization of FeAlPO$_4$-5.

进行, 285 cm^{-1} 处谱峰逐渐消失, 同时骨架铁的谱峰强度逐渐增强. 这表明分子筛晶体结构的形成与铁物种由六配位转化为四配位骨架铁的过程有着密切的关系.

Weckhuysen 课题组的研究表明, 在 CoAlPO$_4$-5 的晶化过程中, Co 的加入为分子筛前体中四元环共顶点的一维链状合成母链添加了一个惰性端基, 较长的六配位 Co^{2+} 中的 Co–O 键长不利于它和其它磷酸铝母链进一步发生反应. 结合不同铁含量的紫外拉曼光谱以及紫外-可见漫反射光谱, 位于 285 cm^{-1} 处 266 nm 激发的拉曼谱峰和高度隔离的六配位 Fe^{3+}物种有关. 在分子筛晶化前, 铁离子以六配位的形式存在, 它为分子筛前体中的一维磷酸铝链添加了一个惰性端基, 六配位的 Fe–O 键不利于它和其它磷酸铝物种发生反应; 当分子筛开始晶化时, 带有铁离子端基的磷酸铝链与其它磷酸铝链进一步发生反应形成分子筛骨架, 六配位的铁离子和邻近的磷酸铝物种反应转化为四配位的骨架铁物种 (见图式 1).

3 结论

利用紫外共振拉曼光谱和紫外-可见漫反射光谱对不同铁含量的 FeAlPO$_4$-5 分子筛进行了研究, 同时研究了分子筛晶化过程中铁物种的变化. 结果表明, 初始凝胶中的 Al/Fe < 380 时, 它们将不能全部进入分子筛的骨架, 一部分将以六配位的 Fe^{3+}物种存在. 不同晶化时间的拉曼光谱和紫外-可见漫反射光谱的结果表明, 与 Fe-ZSM-5 晶化过程中铁物种的变化明显不同: 在 Fe-ZSM-5 晶化过程中, Fe 在初始阶段即与凝胶作用形成具有类似骨架铁的四配位的铁物种; 而 FeAlPO$_4$-5 初始凝胶中的铁物种以六配位的形式存在, 随着晶化的进行逐渐转化为骨架四配位的铁物种. 通过改变凝胶体系的 pH 值或者降低晶化温度等手段可能会降低分子筛的晶化速度, 凝胶前体中的六配位的铁物种有可能会更多地转化为骨架中四配位的铁物种, 提高骨架的铁含量, 从而合成出更高活性的催化剂.

参 考 文 献

1 Wilson S T, Lok B M, Messina C A, Cannan T R, Flanigen E M. *J Am Chem Soc*, 1982, **104**: 1146
2 Jia J F, Wen B, Sachtler W M H. *J Catal*, 2002, **210**: 453
3 Joyner R, Stockenhuber M. *J Phys Chem B*, 1999, **103**: 5963
4 Lobree L J, Hwang I C, Reimer J A, Bell A T. *J Catal*, 1999, **186**: 242
5 Marturano P, Drozdova L, Kogelbauer A, Prins R. *J Catal*, 2000, **192**: 236
6 Sun K, Xia H, Feng Z, van Santen R, Hensen E, Li C. *J Catal*, 2008, **254**: 383
7 Sun K Q, Xia H, Hensen E, van Santen R, Li C. *J Catal*, 2006, **238**: 186
8 赵晓旭, 程党国, 陈丰秋, 詹晓力. 催化学报 (Zhao X X, Cheng D G, Chen F Q, Zhan X L. *Chin J Catal*), 2010, **31**:

68
9 Ren T, Yan L, Zhang X M, Suo J S. *Appl Catal A*, 2003, **244**: 11
10 Raja R, Sankar G, Thomas J M. *J Am Chem Soc*, 1999, **121**: 11926
11 Dugal M, Sankar G, Raja R, Thomas J M. *Angew Chem, Int Ed*, 2000, **39**: 2310
12 Shiju N R, Fiddy S, Sonntag O, Stockenhuber M, Sankar G. *Chem Commun*, 2006: 4955
13 Wei W, Moulijn J A, Mul G. *Microporous Mesoporous Mater*, 2008, **112**: 193
14 Fan W B, Duan R G, Yokoi T, Wu P, Kubota Y, Tatsumi T. *J Am Chem Soc*, 2008, **130**: 10150
15 Dutta P K, Bronic J. *Zeolites*, 1994, **14**: 250
16 Dutta P K, Shieh D C, Puri M. *J Phys Chem*, 1987, **91**: 2332
17 Li C, Xiong G, Xin Q, Liu J K, Ying P L, Feng Z C, Li J, Yang W B, Wang Y Z, Wang G R, Liu X Y, Lin M, Wang X Q, Min E Z. *Angew Chem, Int Ed*, 1999, **38**: 2220
18 Li C. *J Catal*, 2003, **216**: 203
19 Fan F T, Sun K J, Feng Z C, Xia H A, Han B, Lian Y X, Ying P L, Li C. *Chem Eur J*, 2009, **15**: 3268
20 范峰滔, 徐倩, 夏海岸, 孙科举, 冯兆池, 李灿. 催化学报 (Fan F T, Xu Q, Xia H A, Sun K J, Feng Zh C, Li C. *Chin J Catal*), 2009, **30**: 717
21 Fan F T, Feng Z C, Li C. *Acc Chem Res*, 2010, **43**: 378
22 Fan F T, Feng Z C, Li C. *Chem Soc Rev*, 2010, **39**: 4794
23 Li C. *Stud Surf Sci Catal*, 2007, **170**: 561
24 Li C, Xiong G, Liu J K, Ying P L, Xin Q, Feng Z C. *J Phys Chem B*, 2001, **105**: 2993
25 Fan F T, Feng Z C, Sun K J, Guo M L, Guo Q, Song Y, Li W X, Li C. *Angew Chem, Int Ed*, 2009, **48**: 8743
26 Sun K J, Fan F T, Xia H A, Feng Z C, Li W X, Li C. *J Phys Chem C*, 2008, **112**: 16036
27 孙科举. [博士学位论文]. 大连: 中国科学院大连化学物理研究所(Sun K J. [PHD Dissertation]. Dalian: Dalian Inst Chem Phys, Chin Acad Sci), 2009
28 Li L X, Tang X C, Liu H T, Qu Y, Lu Z G. *Electrochim Acta*, 2010, **56**: 995
29 Grandjean D, Beale A M, Petukhov A V, Weckhuysen B M. *J Am Chem Soc*, 2005, **127**: 14454

英 译 文

English Text

The discovery of $AlPO_4$-*n* is regarded as a milestone in the development of molecular sieves [1]. The incorporation of heteroatoms into aluminophosphates has played an important role in enhancing their applications in the fields of adsorption, separation, formation of host-guest advanced materials, and catalysis. Fe-containing molecular sieves have attracted widespread interest because of their unique catalytic properties in a number of reactions, especially in redox catalysis. Fe-ZSM-5 zeolite is especially interesting because of its excellent catalytic performance in environmental catalysis and in selective oxidation etc [2]. Understanding the active sites on Fe-ZSM-5 is important in this field. Generally, the coordinatively unsaturated iron species present in the non-framework positions within the pores of the zeolite are thought to be the active sites [2–8]. However, framework iron is considered to be the active center in the $FeAlPO_4$-*n* catalyst. Ren et al. [9] reported that iron phosphate can serve as a catalyst for benzene hydroxylation with high selectivity exceeding 85% and the Fe(III) ions are tetrahedrally coordinated in the catalyst. The iron atoms are always tetrahedrally coordinated in the framework of the $AlPO_4$-5 structure and they are very good catalysts for several oxidation reactions with molecular oxygen as an oxidant [10,11]. Shiju et al. [12] found that tetrahedral iron atoms in the framework are the active centers during benzene hydroxylation. Wei et al. [13] reported that only when the Fe(III) in the framework is reduced to Fe(II) the catalyst can become active for N_2O decomposition. Thus, information about the framework iron atoms is very important for reactions where $FeAlPO_4$-*n* is the catalyst. However, information on the incorporation of transition metal ions into molecular sieves is difficult to obtain because the amount of metals incorporated into zeolite frameworks is usually very low [14]. UV Raman spectroscopy has been shown to be a powerful tool for the characterization of molecular sieves because of decreased fluorescence and increased sensitivity [15,16]. In addition, because of the resonance Raman effect information about heteroatoms in the framework of molecular sieves can be selectively obtained [17–24].

In this work, UV resonance Raman spectroscopy and UV-Vis absorption spectroscopy were used to investigate $FeAlPO_4$-5 with different iron contents. The evolution of the iron species during the crystallization of $FeAlPO_4$-5 was also studied. The results demonstrate that the iron species transform from a six-coordinated state to a tetrahedral state during hydrothermal crystallization. Some of the iron species cannot enter the framework and they exist in the six-coordinated state when the iron content is relatively high. This work sheds light on the general mechanism of transition metal substituted molecular sieves synthesis.

1 Experimental

1.1 Sample preparation

The aluminum and phosphorus sources were pseudoboehmite (55% Al_2O_3) and H_3PO_4, respectively. Triethylamine (TEA, 99.5%) was used as a SDA. An appropriate amount of H_3PO_4 was stirred with H_2O at room temperature for 30 min followed by the addition of pseudoboehmite. The

mixture was stirred for 120 min and TEA was added to the mixture in a dropwise manner. Finally, the $FeCl_3$ solution was added to the above-mentioned gel and stirred for 120 min. Crystallization was completed in stainless steel autoclaves for 2160 min at 413 K. The solid products were collected by filtration, washed with distilled water, and dried at 353 K.

For the study on the evolution of iron species during hydrothermal crystallization, samples were taken from the autoclaves at different time intervals, collected by filtration, washed with distilled water, and dried at 353 K.

1.2 Sample characterization

XRD patterns were recorded on a Rigaku RINT D/Max-2500 powder diffraction system using Cu K_α radiation (40 kV and 50 mA). UV Raman spectra were recorded on a home-assembled UV Raman spectrograph using a Jobin-Yvon T64000 triplestage spectrograph with a spectral resolution of 2 cm^{-1}. The laser line at 325 nm of an He-Cd laser was used as an exciting source with an output of 50 mW. The power of the laser at the samples was about 1.0 mW. The laser at 266 nm comes from the double-frequency of a DPSS 532 Model 200 532 nm laser.

2 Results and discussion

2.1 Powder XRD patterns and UV-Vis spectra of $FeAlPO_4$-5 with different Al/Fe ratios

Figure 1(a) shows the XRD patterns of $FeAlPO_4$-5 with different Al/Fe ratios, which all exhibit characteristic XRD patterns of AFI topology. Figure 1(b) shows UV-Vis spectra of $FeAlPO_4$-5 with different Al/Fe ratios, which are dominated by one band around 260 nm as a result of oxygen-to-metal (Fe^{3+}) charge transfer (CT). This band is characteristic of Fe^{3+} at the isolated tetrahedral framework sites. With an increase in the iron content, one shoulder band at 290 nm appears and it comes from the isolated octahedral Fe^{3+} complex. This result shows that the amount of Fe^{3+} that can enter the framework is limited.

2.2 Raman spectra of $FeAlPO_4$-5 with different Al/Fe ratios

Figure 2(a) shows the Raman spectra of $FeAlPO_4$-5 with different Al/Fe ratios upon excitation at 266 nm, which is within the range of the charge-transfer bands at 260 nm. Apart from the characteristic bands of the AFI structure at 260, 400, 500, 1140, and 1240 cm^{-1} [25] the UV Raman spectra of $FeAlPO_4$-5 with various iron content exhibit new bands at 630, 1060, and 1210 cm^{-1}. In our previous work [19,26,27], the transitions responsible for these Raman bands were determined by DFT calculations. The bands at 630 and 1060 cm^{-1} were attributed to the symmetric and asymmetric stretching vibrations of $Fe(OP)_4$, respectively. The band at 1210 cm^{-1} was attributed to the symmetric stretching vibrations of FeO_4 because of the asymmetric stretching of the P–O–Al connected with them. However, the symmetric stretching vibrations of FeO_4 cannot be distinguished because framework vibrations (1140 cm^{-1}) appear in the same region. With an increase in the iron content, the intensities of these Raman bands increase. Meanwhile, a new Raman band appears at 285 cm^{-1} and with an increase in the iron content its intensity increase. Combined with the UV-Vis spectra, this band comes from the highly isolated six-coordinated Fe–O vibration [28]. The UV Raman spectra of $FeAlPO_4$-5 with different iron content show that the extra-framework iron species exist even when the iron content is very low. With an increase in iron content the extra-framework iron species increase.

Figure 2(b) shows a plot of the intensity ratio of the band at 630 cm^{-1} over that at 500 cm^{-1} versus the Fe content in $FeAlPO_4$-5. The intensity of the Raman band at 630 cm^{-1} increases with a lowering of the Al/Fe ratio. However, I(630 cm^{-1})/I(500 cm^{-1}) does not increase linearly. The growth rate of the ratio decreases with a lowering of the Al/Fe molar ratio. This result is consistent with the appearance of six-coordinated Fe^{3+} complexes characterized by the UV-Vis spectra of $FeAlPO_4$-5 with a higher iron content. In particular, a six-coordinated Fe^{3+} species appears in the Raman spectrum when the iron content is low.

2.3 Following $FeAlPO_4$-5 formation by XRD and UV-Vis spectroscopy

Figure 3(a) shows the XRD patterns of $FeAlPO_4$-5 (Al/Fe = 760) at different stages of crystallization. The XRD pattern of the sample crystallized for 120 min is indicative of the formation of a small amount of crystals with an AFI structure. Highly crystalline $FeAlPO_4$-5 was obtained after crystallization for 2160 min.

Figure 3(b) shows the UV-Vis spectra of $FeAlPO_4$-5 (Al/Fe = 760) at different stages of crystallization. The UV-Vis spectrum of the precursor shows a broad band at 275 nm, which is a characteristic band of highly isolated six-coordinated Fe^{3+} complexes. With an increase in the crystallization time the band shifts to 260 nm and gradually becomes stronger. The UV-Vis spectrum of the sample that was crystallized for 2160 min shows strong charge-transfer bands at 260 nm. This result suggests that the precursors contain isolated six-coordinated Fe^{3+} complexes. These iron species convert to tetrahedral framework iron gradually during crystallization.

2.4 Following $FeAlPO_4$-5 formation by UV Raman spectroscopy

Figure 4(a) shows UV Raman spectra of $FeAlPO_4$-5 (Al/Fe = 760) excited at 325 nm for different crystallization stages at various times. The Raman spectrum of the initial precursor is characterized by three bands centered at 370, 500, and 1070 cm^{-1}. The Raman bands at 370 and 500 cm^{-1} correspond to vibrational modes of the isolated octahedral AlO_6 species of pseudoboehmite. The Raman band at 1070 cm^{-1} is assigned to the amorphous Al–O–P species. With an increase in crystallization time the intensities of the Raman bands at 370 and 500 cm^{-1} decrease indicating the consumption and reaction of the octahedral AlO_6 species. With prolonged synthesis, three Raman bands at 741, 899, and 1010 cm^{-1} appear. These are characteristic bands of protonated TEA. After 120 min, two Raman bands at 260 and 500 cm^{-1} appear and their intensities increase in parallel. These two bands are assigned to channel breathing vibrational modes and deformations involving the four-membered rings, respectively. The appearance of the Raman band at 260 cm^{-1} indicates that the synthesis gels are partially crystallized. Moreover, a shoulder band at 1140 cm^{-1} appears. This band is assigned to coupled symmetric stretching modes of individual PO_4 and AlO_4 tetrahedra in which adjacent tetrahedra vibrate in an antiphase. The appearance of this Raman band is further evidence that the molecular sieve has crystallized.

To investigate the evolution of iron species during the synthesis of $FeAlPO_4$-5, the process was monitored by UV Raman spectroscopy with excitation at 266 nm. Figure 4(b) shows the Raman spectra obtained upon excitation at 266 nm for $FeAlPO_4$-5 (Al/Fe = 760) at different stages of crystallization. The Raman spectra of the samples crystallized for 0–120 min show characteristic bands of pseudoboehmite at 370 and 500 cm^{-1} as well as a comparatively weak band centered at 285 cm^{-1}. The appearance of the Raman band at 260 cm^{-1} indicates that the synthesis gel was partially crystallized. Meanwhile, Raman bands associated with framework iron at 630, 1060, and 1210 cm^{-1} appear. With increasing crystallization time the intensities of these bands increase and the band at 285 cm^{-1} decreases. This result demonstrates that the transformation of iron from an octahedral state to a tetrahedral state is closely associated with the formation of the framework.

Grandjean et al. [29] reported that the Co^{2+} ions hinder the crystallization of $CoAlPO_4$-5. It is most likely that this is related to the requirement for Co^{2+} ions to transform from octahedral to tetrahedral geometry before crystallization. Combined with the UV-Vis and the UV Raman spectra of $FeAlPO_4$-5 with different iron content the Raman band at 285 cm^{-1} arises from the octahedral isolated iron species. In the precursor gel the iron species exist in the form of an octahedral isolated state. A longer Fe–O bond hinders its reaction with other $AlPO_4$ species. Upon the initiation of crystallization the 1-dimensional $AlPO_4$ chains containing iron react with other $AlPO_4$ chains nearby to form the framework. Meanwhile, the octahedral isolated iron atoms react with the $AlPO_4$ species to transform into tetrahedral framework iron (Scheme 1).

3 Conclusions

UV Raman spectroscopy and UV-Vis spectroscopy were used to study $FeAlPO_4$-5 with different iron content and the evolution of iron species during the crystallization of $FeAlPO_4$-5. The results show that not all the iron enters the framework when the Al/Fe ratio in the precursor gel is lower than 380. Part of the iron exists in the form of an octahedral isolated state. The results of the UV Raman and UV-Vis spectra of $FeAlPO_4$-5 at different stages of crystallization indicate that the evolution of iron during the crystallization process is different from that of Fe-ZSM-5. In the precursor gel of Fe-ZSM-5 the iron reacts with the gel to form tetrahedral iron species, which is similar to the framework iron species. However, the iron in the precursor of $FeAlPO_4$-5 exists in the octahedral state. With the initiation of crystallization the octahedral isolated iron atoms transform into the tetrahedral state in the framework. It is suggested that methods such as adjusting the pH or decreasing the crystallization temperature would decrease the crystallization rate. In such a way, the octahedral isolated iron atoms might have enough time to enter the framework and increase the amount of lattice iron atoms.

Full-text paper available online at Elsevier ScienceDirect
http://www.sciencedirect.com/science/journal/18722067